Fluxionality of gold nanoparticles investigated by Born-Oppenheimer molecular dynamics

Angelo Vargas,[1,*] Gianluca Santarossa,[1] Marcella Iannuzzi,[2] and Alfons Baiker[1]
[1]*Institute for Chemical and Bioengineering, Department of Chemistry and Applied Biosciences, ETH Zurich, Hönggerberg, HCI, 8093 Zurich, Switzerland*
[2]*Institute of Physical Chemistry, University of Zurich, Winterthurerstrasse 190, 8057 Zurich, Switzerland*
(Received 13 August 2009; published 25 November 2009)

The structure and electronic properties of gold nanoparticles (Au 12, Au 13, Au 14, Au 15, Au 20, Au 34, and Au 55) have been investigated using Born-Oppenheimer *ab initio* molecular dynamic simulations of 50 to 80 ps in order to have an insight in the recently proposed fluxional character of nanosized gold. The dynamic changes in shape, symmetry, and atomic coordination of atoms within clusters, occurring in the time scale of picoseconds, which are characteristic of fluxionality, have been investigated for all the above systems at 300 K. Except for Au 20, all systems have been found to have fluxional properties. The extent and the type of fluxional behavior changed according to the number of atoms constituting the particle. At 300 K Au 12 and Au 13 rapidly generate several different topologies which cyclically interconvert. Au 14 shows a rotation of 8 external gold atoms around a core of six atoms. Au 15 is more rigid, but interestingly shows the interconversion between enantiomeric structures within the time scale of the simulation. Au 20 shows a high stability of the pyramidal topology and is the only one of the investigated systems not to show fluxionality within the assigned temperature and time scale. Au 34 and Au 55 show fluxionality of the outer shell and within the sampled time scale are able to change coordination of the outer shell atoms and thus open and close surface holes. For all the particles in study the structures forming the local minima were isolated and separately optimized, and the electronic properties of the thus obtained structures were analyzed.

DOI: 10.1103/PhysRevB.80.195421 PACS number(s): 61.46.Bc, 61.25.Mv, 61.20.Ja

I. INTRODUCTION

There has been a great interest for the chemistry and physics of metal nanoparticles in recent years.[1–3] In particular the chemistry of small gold particles has attracted much attention and its theoretical properties have been extensively reviewed.[4–7] Such interest originates from several reasons: the special catalytic activity of small clusters as compared to larger ones,[8–10] possible application in the building of nanoscale devices,[11–13] the special properties as semiconductors,[14,15] biosensors,[16] electrodes,[17] and their optical properties.[16,18,19] In general when the dimensions of metal particles are reduced to a size comparable to that of the constituent atoms, their electronic structure deviates dramatically from that of the bulk metal. This phenomenon has very relevant effects on both physical and chemical properties of the metal.[14,20,21] In the field of catalysis one particularly striking phenomenon underlying the special properties of size and shape dependence of materials is the ability of finely dispersed gold to catalyze oxidation reactions.[22,23] Bulk gold is in fact extremely inert and has been known and used as such throughout the history of materials. The inertness of bulk gold is the origin of the so-called "nobility," or resistance to oxidation, of this metal. An interesting theoretical basis for the nobility of gold has been given by Hammer and Nørskov based on electronic structure calculations,[24] while other theoretical and experimental studies have investigated the origin of the decrease in nobility of gold.[25,26] Several studies have been published that aim at understanding the origin of the special reactivity of nanosized gold particles toward oxygen,[21,25,27–34] but one of the keys to the understanding of the peculiar reactivity of small gold clusters lies in its fluxional character, since structural isomers are in principle able to adapt their structures toward the most favorable free-energy path.[25,35] Nonetheless only few contributions are present in the literature concerning the fluxionality of gold particles.[35–38] In general, a detailed understanding of the relation between structure and properties of gold nanoparticles could lead to the tailoring of electronic properties such as optical, redox, and chemical behavior.

Born-Oppenheimer molecular dynamics (BOMD) is a very refined tool for the theoretical investigation of dynamical phenomena in metal cluster.[25,39–42] In the present investigation we have studied the dynamics of interconversion, the structural and electronic properties of gold nanoparticles in the size range of 0.5–1.0 nm (Au 12, Au 13, Au 14, Au 15, Au 20, Au 34, and Au 55) using BOMD. Nanosized gold particles have been shown to possess a range of structures lying in a close energy range and to be fluxional at room temperature in the time scale of a few tens of picoseconds. The remarkable property of fluxionality for gold nanoclusters[36,38] is consistent with the structural instability of ultrafine metal particles observed by Iijima and Ichihashi and by Ajayan and Marks.[43,44] In our study fluxionality in the picoseconds regime, corresponding to the time scale of chemical reactivity, has been described for all the investigated systems, and local minima associated with specific numbers of atoms have been isolated and their geometrical and electronic properties have been analyzed and discussed.

II. COMPUTATIONAL METHODS

Gaussian and plane wave (GPW) formalism[45,46] as implemented in the CP2K code[47] has been used for the BOMD simulations and for geometry optimizations within the same level of theory in terms of Hamiltonian, basis sets and pseudopotentials. In addition zero-order regular approximation (ZORA) relativistic Hamiltonian[48,49] has been used as implemented in the Amsterdam density functional (ADF)

code[50] for geometry optimizations and the study of relativistic effects on cohesion.

A. Gaussian and plane-wave calculations

We use the latest implementation of the GPW formalism in the quickstep module of the CP2K program package, a suite of programs aimed at performing efficient electronic structure calculations and molecular dynamics at different levels of theory.[51] The Kohn-Sham orbitals are expanded in terms of contracted Gaussian type orbitals (GTO),

$$\psi_i(\mathbf{r}) = \sum_{\alpha} C_{\alpha i}\varphi_{\alpha}(\mathbf{r}), \tag{1}$$

where ψ_i is the molecular orbital corresponding to the i-th Kohn-Sham state, $\{\varphi_\alpha\}$ are the basis set functions, and $\{C_{\alpha i}\}$ the expansion coefficients. The auxiliary PW basis set is, instead, used only to expand the electronic charge density for the calculation of the Hartree potential. In order to limit the number of PW functions, the interaction of the valence electrons with frozen atomic cores is described via the use of norm-conserving, dual-space-type pseudopotentials.[52] In particular, we used a pseudopotential (PP) including all the electrons up to the $5p$ levels in the core, thus treating the 11 electrons, corresponding to the $5d$ and $6s$ levels, explicitly in the valence. The GTO basis set has been optimized for the specific Au-PP. We found that the double-ζ valence basis set, based on the Mol-Opt method[53] is apt for the description of gold. For the auxiliary PW expansion of the charge density, the energy cutoff has been set at 180 Ry. The exchange and correlation term was modeled using the Perdew-Burke-Ernzerhof (PBE) functional.[54] For the solution of the self-consistent field (SCF) equations, we used an optimizer based on orbital transformations, which scales linearly in the number of basis functions.[55] It has been already demonstrated that this optimization algorithm, in combination with the GPW linear scaling calculation of the Kohn-Sham matrix, can be used for applications with several thousands of basis functions.[56] Geometry optimizations have been carried out using the Broyden-Fletcher-Goldfarb-Shanno minimization algorithm,[57–61] and the structures have been optimized until the atomic displacements were lower than 3×10^{-3} Bohr and the forces lower than 4.5×10^{-4} Ha/Bohr. The clusters were modeled by means of perfect polyhedra of increasing size from 13 to 55 Au atoms, with icosahedral shapes. The initial Cartesian coordinates were set according to the Au-Au distance of the bulk (2.977 Å) and all the atoms were set free to relax to their equilibrium positions. The clusters were included into cubic cells of different sizes in order to leave approximately 5 Å of free space in the three directions of space for each molecule, and no periodic boundary conditions were applied during the molecular dynamics and molecular optimizations. Each molecular dynamics simulations have been run for 60–80 ps. A time step of 1 fs, a wave function convergence of 10^{-5} guarantee energy conservation during the dynamics. The sampling of the canonical ensemble at 300 K is obtained by coupling to a thermostat using the canonical sampling through velocity rescaling scheme[62] with a time constant of 1000 fs. On 16 processors (Sun Blade 6048 Modular Systems, each blade containing four quadcore AMD Opteron 2380 processors, "Shanghai" core 2.5GHz, 6 MB L3-cache, 32 GB of shared memory) 1 ps of dynamics simulation of the Au 13 nanoparticle takes approximately 5.2 h. For Au 55 1 ps of dynamics simulation takes approximately 39 h.

B. ZORA calculations

ZORA calculations were performed using the ADF program package.[50] The local part of the exchange and correlation functional was modeled using the VWN (Vosko, Wilk, Nusair) parameterization of the electron gas.[63] For the nonlocal part of the functional the PBE functional was used.[54]

Relativistic effects were taken into account using a ZORA Hamiltonian as implemented by van Lenthe *et al.*[48,49] Furthermore atoms were modeled using a frozen core approximation (core electrons were frozen up to $4f$ for Au) where the core was modeled using a relativistically corrected core potential. This was calculated within an X-α approximation (without gradient corrections) but with the fully relativistic Hamiltonian, including spin-orbit coupling. The ZORA formalism requires a special basis set, including much steeper basis functions.[64] Within this basis set, a triple-ζ plus polarization functions basis set was used for gold.

C. Grimme correction

The effect of dispersion forces in the calculation of the cohesive energies of gold nanoparticles was investigated using the B97-D density functional proposed by Grimme[65] based on the Becke '97 power series. It was shown that the performance of this functional for noncovalently bound systems, including many pure van der Waals complexes, reaches the average CCSD(T) accuracy.[65]

D. Post processing

1. Cohesive energy

The cohesive energies (C_{En}) have been calculated as the difference between the total energy per atom and the energy of the single atom, that is:

$$C_{En} = E_{Cluster}/N_A - E_{Atom},$$

where $E_{Cluster}$ is the total energy of the particle, N_A is the number of atoms in the particle and E_{Atom} is the energy of the isolated atom.

2. Root-mean-square displacement

The root-mean-square displacement (RMSD) was calculated using the following formula:

$$\mathrm{RMSD} = \sqrt{\frac{\sum_i (x_i - x_i^R)^2}{N_A}},$$

where x_i are the coordinates of atom i, N_A is the number of atoms in the particle, and x_i^R are the coordinates of the reference frame.

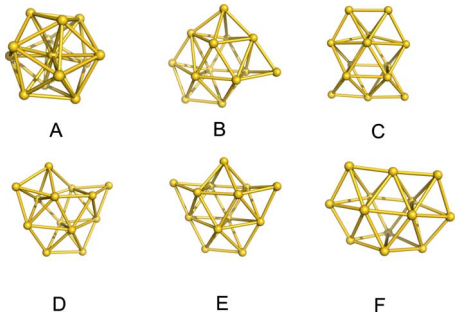

FIG. 1. (Color online) Three-dimensional minimum energy structures of Au 13 that are formed during 80 ps of MD simulation at 300 K.

3. Coordination number

The coordination number was calculated using the following formula:[66–68]

$$C_{A,B} = \sum_{i=1}^{N_A} \left[\sum_{\substack{j=1 \\ j \neq i}}^{N_B} \frac{1 - \left(\frac{r_{ij}}{R_{AB}} \right)^p}{1 - \left(\frac{r_{ij}}{R_{AB}} \right)^q} \right], \quad q > p,$$

where N_A and N_B are the numbers of atoms involved, r_{ij} is the interatomic distance, and R_{ab} is the cutoff distance that measures the bond length. p and q determine the decay of the function. The cutoff value R_{AB} was set to 3.4 Å while p and q have been set to 10 and 16, respectively.

III. RESULTS AND DISCUSSION

A. Au 13

Number 13 is the first term of the Mackay series of icosahedra. Members of this series (13, 55, 147, etc.) are found by adding a layer to the icosahedron, and the resulting numbers of atoms are often referred to as "magic numbers," indicating special values that correspond to possible stable structures. Icosahedra of this series are commonly taken as reference structures for nanoparticles since they posses a high symmetry, and they are the closest tradeoff between a spherical arrangement of the atoms and the fcc structure of the bulk solid. A molecular dynamics (MD) simulation has been run starting from an optimized icosahedral structure of an Au 13 nanoparticle (Fig. 1(A)). The trajectory of the simulation was studied and those structures were identified that were stable for at least a few picoseconds or possessed a special symmetry. These were separately optimized and actually corresponded to local minima (Fig. 1, Cartesian coordinates available as auxiliary material).[69] Some technical details of the computational times involved in the dynamic simulation have been added in the section dedicated to the "computational methods" section, in order to give an idea of their feasibility. Figure 1 shows the five three-dimensional structures (B-F) that were found within 80 ps of molecular dynamics at 300 K and Fig. 2 shows the evolution of those structures at the same temperature on a graphic of the total energy vs time (ps) during 80 ps of molecular dynamics. The most relevant features of the dynamics simulation are illustrated in the following sections.

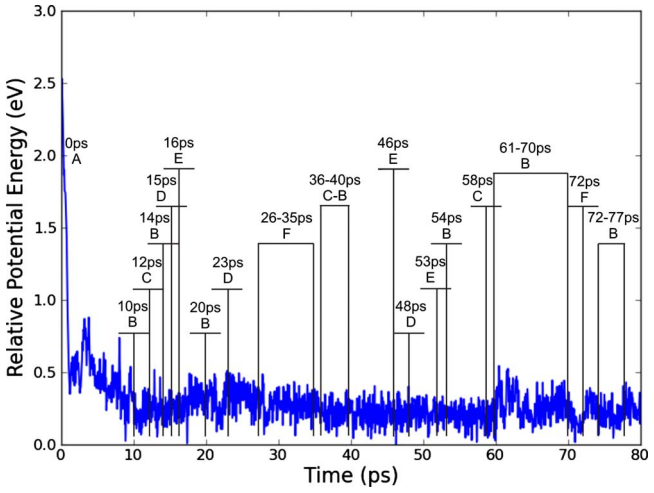

FIG. 2. (Color online) Evolution of the Au 13 structures during 80 ps of MD simulation at 300 K, above a plot of relative energy. Letters A, B, C, D, E, and F refer to the structures in Fig. 1.

1. Evolution of the structures during the MD

A molecular dynamic run at 300 K caused a rapid collapse of the symmetric structure of the icosahedron (A), and the successive formation of five three-dimensional structures (B-F, in Fig. 1). Approximately the first 10 ps of MD can be considered as the equilibration time of the simulation. During this time the initial icosahedral structure evolves to the equilibrated geometries. Such structures are characterized by having a core-free or cage-like structure. The preference of gold for cage-like structures has been noted by several researchers.[41,70–72]

2. Fluxionality

Au 13 has a fluxional structure.[35–38] Many local minima, very close in energy and interconvertible through low lying energy barriers, coexist at 300 K. The substantially flat energy observed after the first 10 ps (Fig. 2) indicates that the structures are very close in energy, while the facile interconversion at room temperature shows that energy barriers between them are below K_BT. This kind of behavior is characteristic of fluxionality. Figure 3 shows the same scheme of interconversion between structures, over a graphic of the RMSD of the coordinates. It must be noted that when analyzing the RMSD we should focus on the local changes in the graph while different heights do not necessarily represent different structures. In fact RMSD is an average distance from a reference conformation, the atoms of which must be labeled. Due to fluxional behavior, the position of the labeled atoms changes, and as a consequence the RMSD values cannot be correlated with a particular topology, but only to a local change in topology. It can, and indeed does occur, that identical topologies have different RMSD value. It was thus chosen to take structure D as reference topology because the resulting changes in this descriptor well reproduce the passages from one structure to the other. Thus RMSD allows following the structural evolution of Au 13 although the energy of all structures is very close.

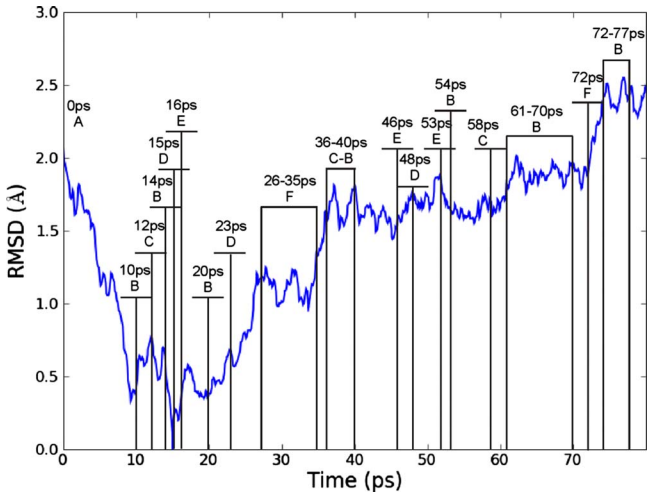

FIG. 3. (Color online) Evolution of the Au 13 structures during 80 ps of MD simulation at 300 K, above a graph of RMS displacement. The reference structure is the one at 15 ps. Letters A, B, C, D, E, and F refer to the structures in Fig. 1.

3. Local minima

The topologies identified in the explored conformational basin [Figs. 1(B)–1(F)] are consistent with the minimum energy structures identified by Xiao *et al.*,[71] who based their investigation on a trial-and-optimization approach extended to many guess structures. In other words starting the simulation from an icosahedral geometry leads the system to the correct set of three-dimensional (3D) minimum energy structures. This does not in principle guarantee that all the possible 3D structures are identified, but it is observed that the ones that belong to the sampled basin [Figs. 1(B)–1(F)] have the lowest energy (among 3D structures) within the ones described in literature. It should also be noted that some of the topologies within this basin are not present in the existing literature, and that therefore our approach has allowed the identification of some low-energy conformations for Au 13. Nonetheless the MD simulations show that a static analysis of the single minima is incomplete, while a dynamic description in terms of the coexistence of minima within a (local) basin in a free-energy landscape provides a more accurate picture of the cluster behavior. In fact at room temperature Au 13 is in a liquid phase characterized by the coexistence and continuous interconversion between all of the identified shapes.

4. Instability of the icosahedral structure

It is striking that the icosahedral structure for Au 13 is not a stable topology. In fact the icosahedron is a very bad guess for Au 13, and its structure is surpassed in stability by all others found. This can be clearly seen by the sharp drop in the energy (Fig. 2) and by the sharp change in RMSD (Fig. 3) within the first ps of the dynamic simulation. This is in contrast to the findings of Doye and Wales[73] using Sutton-Chen potentials[74] coupled with either Li and Scheregas's Monte Carlo minimizations[75] or basin-hopping algorithm. According to their investigations Au 13 icosahedron is a global minimum, which could have been expected due to the fact that Sutton-Chen potentials are embedded atom model (EAM) type potentials. DFT calculations[71,76] on the other hand are in full agreement with our findings showing that the use of empirical potentials is still problematic for the conformational study of clusters of heavy elements.

5. 3D/2D transition

A dynamic simulation of 80 picoseconds at 300 K was able to identify several three-dimensional structures of Au 13, while bidimensional flat structures were nonaccessible within this time scale. The conversion between two-dimensional (2D) and 3D structures of a gold cluster requires a high activation energy. In fact Koskinen *et al.*,[37] based on a density-functional tight-binding model[77] have calculated an activation barrier between 2D and 3D fluxional structures of approximately 0.8 eV at 0 K. Although lying at lower energy, the flat conformations have low probability to be accessed starting from three-dimensional structures. This transition would require the sampling of a much longer time at 300 K. We are currently investigating methods of enhanced sampling to address the problem of the 2D/3D phase transition.

6. Phase-space diagrams

The structures found by molecular dynamics appear cyclically. They are transformed and reformed within a time scale of tens of picoseconds. Atoms in clusters are continuously shuffled and change position within an even shorter typical time. Figure 4(A) shows a diagram of a phase space defined by a structural descriptor d, sum of the distances of the neighboring atoms in each structure ($\Sigma_{i\neq j} d_{ij}$), and the energy of each structure. It shows that not all structures are able to interconvert. The passages, E→C and F→E are mediated by other structures. In particular it should be noted that F, though very close in energy to E, is never directly accessed from E but needs to pass through structure D. And also E and C are close in energy but do not directly interconvert. Figure 4(B) shows a diagram where the position of the structural labels B, C, D, E, and F are arbitrarily posed on a pentagon. The dynamic simulation starts from A (icosahedron) and evolves irreversibly to the network of interconnections in the graph. The dashed lines represent passages which are not allowed. As descriptor of dynamic transformations each particle should have a unique graph of interconnections at a given temperature.

7. Electronic properties

Table I summarizes the properties of the isolated minima found during the dynamic simulation. Note that the second column in the Table I gives the energy differences between the structure and the most stable structure of the examined series, so that increasing values reflect larger instabilities. Thus the values of ΔEn provide an order to structures in terms of their relative total energy. Icosahedral Au 13 is ca 2.6 eV less stable than the other structures and is associated to the lowest highest occupied molecular orbital (HOMO)-lowest unoccupied molecular orbital (LUMO) (H-L) gap and the lowest cohesive energy while structure D has the lowest energy. It is striking that such particles do have an H-L gap,

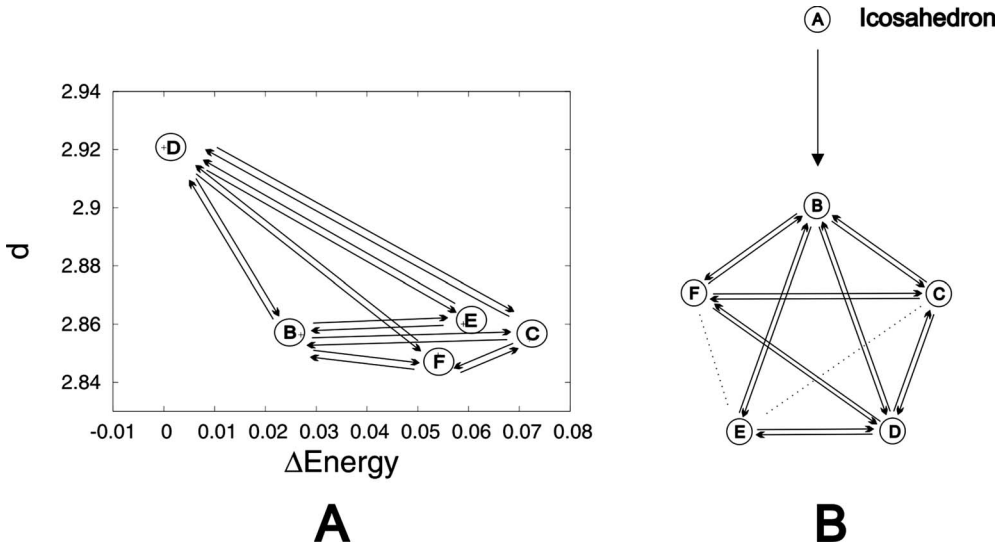

FIG. 4. Network of the dynamic of interconversion between three-dimensional Au 13 nanoparticles: (A) diagram in the phase space defined by the structural descriptor *d* and by the Δ Energy (eV, as by Table I), and (B) scheme of the interconnection network, with solid lines indicating possible interconversions and dotted lines indicating interconversions between structures that do not occur at room temperature within the sampled time.

indicating a strong deviation from the metallicity of the bulk. With the exception of the icosahedral geometry the H-L gap is virtually insensitive to the structural changes. In fact H-L gaps are very close in energy (to less than 0.02 eV) for all the equilibrium structures. Cohesive energies have been investigated for all the minimized structures. Since it has been proposed that structure and bonding in gold particles have a large relativistic component,[78,79] each structure was separately reoptimized using ZORA relativistic Hamiltonian (see computational methods). Indeed the ZORA formalism revealed higher cohesive energies, meaning that addition of spin-orbit interaction, mass-velocity, and Darwin terms to the Hamiltonian does add some energy to the cohesion. Nonetheless also the nonrelativistic Hamiltonian associated with the CP2K geometry optimizations and molecular dynamics runs are in very good agreement with the ZORA results, giving the same minimum energy structures and following the same order in energy.

It seems that most of the energy is recovered also with the nonrelativistic Hamiltonian. ZORA calculations regularly give about 5% increase in the value of C.En. This is likely due to the inclusion of the relativistic effects at the level of the description of the pseudopotential in the CP2K calculations. Cohesive energies have also been calculated using the B97-D density functional proposed by Grimme,[65] which showed that the contribution from dispersion forces amounts to about 2% of the total cohesive energy.

B. Au 12

The dynamic simulation of Au 13 shown in the previous paragraph showed that the icosahedral structure is not stable, while cage-like structures interconvert with low-energy barriers. We removed one atom from the Au 13 C structure in Fig. 1 and generated, after geometry optimization, structure A in Fig. 5. Starting from this geometry we let the dynamic simulation run for 80 ps, thus generating structures B to F in Fig. 5 (Cartesian coordinates available as auxiliary material).[69] Most relevant features of the particle dynamics were: (i) As for Au 13, the conformational basin sampled includes the most stable geometries for Au 12 according to literature,[71,80] and adds more low-energy structures to the ones described until now. (ii) As for Au 13 the particle was fluxional and five different geometries could be generated at room temperature within the picoseconds time scale. We have mentioned above that the basin is the correct one (comprising the lowest energy 3D Au 12 structures). We should note that according to literature structure E in Fig. 5 is the most stable, while the MD simulation shows that at room temperature this is simply one of the coexisting structures which rapidly interconvert. In fact as before it would be more correct to state that at room-temperature Au 12 does not have a fixed topology but is in a liquid phase and its structure oscillates between topologies that are local minima in the reference potential-energy surfaces. (iii) Closed (B and D) or open (C, E, and F) cages were generated. (iv) The structural patterns found, i.e., four Au atoms displayed at the vertices of a regular tetrahedron, were similar to those already found for Au 13, showing that there are regular patterns for Au assemblies. (v) The phase-space diagram [Fig. 6(A)] has a simpler structure, with less interconnection. Also for Au 12 lower energy structures (e.g., F) are not directly accessible from all other but require the passage from other transition structures. For the static properties it should be noted that all isolated particles deviate from the metallicity of the bulk by showing an HOMO-LUMO gap. Interestingly the H-L gaps are larger than the ones found for Au 13. The most stable structure (E, Fig. 5) has the smallest H-L gap but there is no clear correlation between total energy and this electronic indicator. The details of the electronic structures seem dependent on the shape rather than on the total energy, which indicates that the electronic properties are influenced by the shape.

TABLE I. Electronic properties of the minimum energy structures of Au particles. The letters in the first column refer to structures in Figs. 1, 5, 7, 10, 11, 13, and 15. The second column lists the differences of total energies (ΔEn.) relative to the most stable structure (zero energy in the table); the third column lists the point groups (PG); the fourth column lists the HOMO-LUMO gap (H-L gap); the fifth, sixth, and seventh columns list the cohesive energy (CEn) calculated with the PBE functional, calculated with the PBE functional plus zero order regular approximation to account for relativistic corrections (see computational methods) (Refs. 48 and 49), and calculated with the PBE functional plus the Grimme correction for dispersion forces (Ref. 65), respectively. All energy values are in eV.

	ΔEn.	P. G.	H-L gap	CEn (PBE)	CEn (ZORA)	CEn (Grimme)
			Au 12			
A	0.357	$\mathcal{C}_{2v}$	1.12	1.95	2.06	2.01
B	0.358	$\mathcal{C}_{2v}$	1.13	1.95	2.06	2.01
C	0.190	$\mathcal{C}_1$	1.21	1.97	2.08	2.02
D	0.102	$\mathcal{C}_{2v}$	1.13	1.97	2.09	2.03
E	0.000	$\mathcal{C}_{2v}$	0.97	1.98	2.10	2.04
F	0.112	$\mathcal{C}_s$	1.33	1.97	2.09	2.03
			Au 13			
A	2.626	$\mathcal{I}_h$	0.12	1.79	1.90	1.85
B	0.027	$\mathcal{C}_s$	0.20	1.99	2.10	2.04
C	0.072	$\mathcal{C}_{2v}$	0.18	1.98	2.10	2.04
D	0.000	$\mathcal{C}_s$	0.20	1.99	2.10	2.05
E	0.059	$\mathcal{C}_{2v}$	0.18	1.98	2.10	2.04
F	0.054	$\mathcal{C}_{2v}$	0.18	1.98	2.10	2.04
			Au 14			
A	0.000	$\mathcal{C}_{2v}$	1.55	2.05	2.18	2.11
A′	0.596	$\mathcal{C}_1$	0.56	2.01	2.13	2.07
B′	0.740	$\mathcal{C}_1$	0.90	2.00	2.12	2.06
			Au 15			
A	0.229	$\mathcal{C}_1$	0.18	2.03	2.15	2.09
B	0.020	$\mathcal{C}_1$	0.16	2.05	2.17	2.11
C	0.020	$\mathcal{C}_1$	0.16	2.05	2.17	2.11
B′	0.000	$\mathcal{C}_1$	0.16	2.05	2.17	2.11
C′	0.004	$\mathcal{C}_1$	0.16	2.05	2.17	2.11
			Au 20			
		$\mathcal{T}_d$	1.81	2.21	2.34	2.27
			Au 34			
A	0.165	$\mathcal{C}_1$	0.95	2.32	2.46	2.39
B	0.000	$\mathcal{C}_1$	1.13	2.32	2.46	2.40
C	0.022	$\mathcal{C}_1$	1.08	2.32	2.46	2.39
D	0.142	$\mathcal{C}_1$	1.15	2.32	2.46	2.39
			Au 55			
A	0.929	$\mathcal{C}_s$	0.05	2.39		2.47
D	0.000	$\mathcal{C}_1$	0.05	2.40		2.48

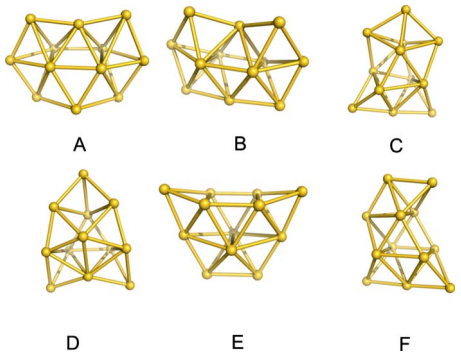

FIG. 5. (Color online) Three dimensional minimum energy structures of Au 12 that are formed during 80 ps of MD at 300 K.

C. Au 14

The starting structure of an Au 14 nanoparticle was built from structure F of Au 13 (Fig. 1) by addition of a single atom. The obtained structure was optimized previous to running the dynamic simulation. Figure 7(A) shows the obtained particle shape (Cartesian coordinates available as auxiliary material).[69] It should be noted that this particles shape corresponds to the lowest-energy Au 14 particle found[71,81] and that therefore the MD is sampling the lowest energy basin for 3D Au 14 structures. Figure 8 shows the evolution in time of such structure against the potential energy. The basic topology remains constant during the 60 ps MD. Nonetheless during the simulation the atoms constituting the particle change their position, in particular the eight atoms surrounding the central core rotate around the six central atoms as shown in Fig. 9. A complete rotation occurs in about 5 ps. The images in Fig. 9 are less symmetric than structure A in Fig. 7 because they are snapshots from the dynamic simulation and are not geometrically optimized as structure A. During the MD the potential energy remains almost constant. Interestingly the fluxionality of this nanoparticle does not lead to different particle shapes but simply leads to a constant rotation of the external atoms within the same shape. This particle has a distorted $\mathcal{C}_{2v}$ symmetry and a cage-like structure as seen for Au 12 and Au 13. In order to test another conformational basin and verify whether other topologies were accessible by MD, another trial structure for Au 14 was built by addition of two atoms to structure B of Au 12 (Fig. 5). The structure was optimized leading to A′ (Fig. 7). The dynamic simulation shows that A′ is quite stable and only at 38 ps it is transformed to B′ to rapidly evolve back (after 6 ps) to A′. Note that this simulation run samples a basin at higher energy than the previous one (Fig. 8, Table I). Also this topology is cage-like as the previous one, but it loses symmetry and drops to point group $\mathcal{C}_1$ being therefore chiral. Chirality seems a frequently occurring phenomenon for gold clusters and has been observed by several researchers.[82–90]

Within the sampling time and at 300 K at which the dynamic simulations were run the conformational spaces of A and A′-B′ do not mix, meaning that the barrier to overcome to switch from one to the other structures is higher that K_bT. As stated above they seem to belong to different basins in the conformational space of Au 14 nanoparticles. Structures A′ and B′ are more open than A, and it would be tempting to ascribe their lower stability to such feature since open structures have a larger proportion of lower coordinated metal atoms. But if we observe the energies of the various shapes of Au 12 and Au 13 it can be seen that for those particles more open structures are also more stable. It seems that for gold openness and closeness, level of saturation of metal atoms and coordination number cannot be valid structural criteria to be correlated with the total energy. As for Au 12

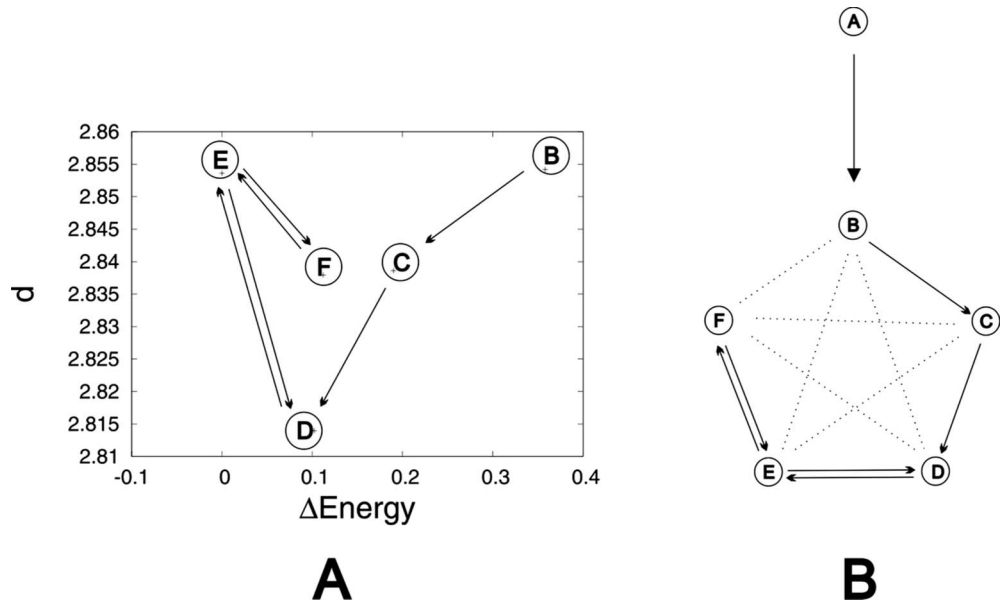

FIG. 6. Network of the dynamic of interconversion between three-dimensional Au 12 nanoparticles: (A) diagram in the phase space defined by the structural descriptor *d* and by the Δ Energy (eV, as by Table I), and (B) scheme of the interconnection network, with solid lines indicating possible interconversions and dotted lines indicating interconversions between structures that do not occur at room temperature within the sampled time.

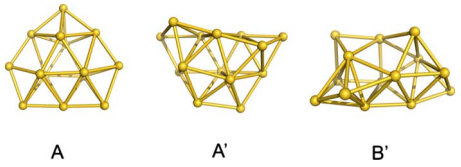

FIG. 7. (Color online) Three dimensional minimum energy structures of Au 14 that are formed during 60 ps of MD at 300 K.

and Au 13, also Au 14 particles largely deviate from the metallicity of the bulk since they are characterized by a H-L gap (Table I). In this particular case the lowest energy structure [Fig. 7(A)] has the highest H-L gap. Also in this case the absolute values of H-L gap are larger than those found for Au 13. Cohesion energies follow the trend of the total energy as expected. Interestingly the values of H-L gap and cohesive energies of structure A are especially high as compared to those found for Au 12 and Au 13.

D. Au 15

The starting point of the dynamic simulation of an Au 15 particle was structure A of Au 14 (Fig. 7), with the addition of one atom. This generated at first structure A for Au 15 [Fig. 10(A)]. This, as well as the other topologies which were formed during the MD (Fig. 10, Cartesian coordinates available as auxiliary material),[69] present the basic structure of Au 14 A with an additional gold atom (that we here call "peripheral") that does not disrupt the basic structure. B, C, B′, and C′ are lower-energy structures than A, and the latter exists only for 3 ps during the first part of the simulation. For the rest of the sampling time B, C, B′, and C′ interconvert. The rotation of the external atoms of the cluster is not observed for Au 15 during the simulation time, but it is interesting to note that B and C (or B′ and C′) are enantiomeric structures. B possesses the same topological connections as B′, differing from B′ for a slight relative rotation of the

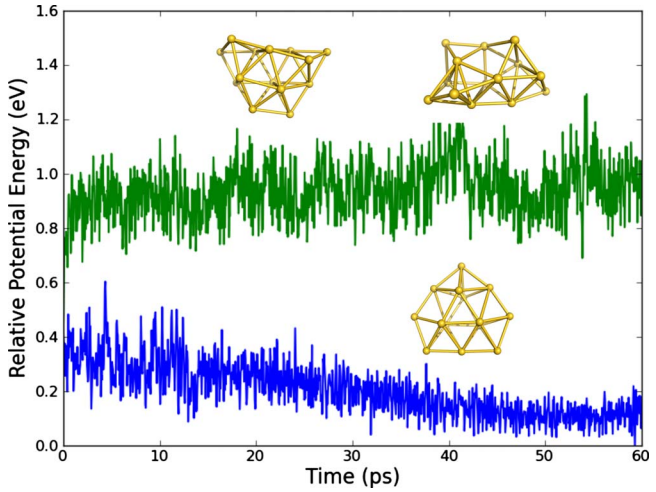

FIG. 8. (Color online) Evolution of two Au 14 structures starting from different initial geometries during two MD simulations of 60 ps each, at 300 K. The two basins at lower (below in the graphic) and higher (above in the graphic) energies do not mix.

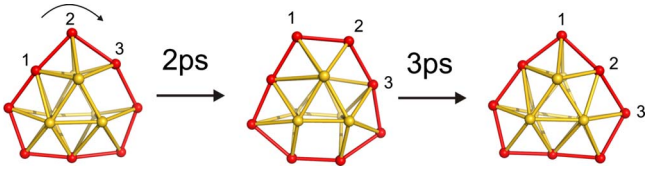

FIG. 9. (Color online) Rotation of the outer crown of gold atoms in an Au 14 particle. The central core of six gold atoms is fixed while the outer eight rotate around them in the time scale of about 5 ps.

triangles forming the core. The same observation is valid for C and C′. Interestingly, the distorted B′ and C′ geometries are more stable than B and C. Although B and B′ are different minima they interconvert within the picosecond time scale, showing that the energy barrier to overcome is lower than K_bT. The interconversion between enantiomeric structures B and C (or B′ and C′) occurs in the time scale of tens of ps. These geometries are characterized by the presence of a peripheral atom not belonging to the external crown of the structure. The enantiomeric conversion takes place when the peripheral atom enters the structure and at the same time an atom from the external crown takes its place. This shows that the fluxionality indeed still exists, but in a different form as observed for Au 14. The peripheral atom thus enters and exits the external crown, this process seemingly having a lower activation barrier than the rotation of the crown itself. It is of relevance to observe that a similar concerted effect has been reported by Akola and Manninen for Al 14, although at higher temperature.[91] Note that the enantiomeric structures have slightly different energies, which is attributed to the computational accuracy which is in the range of the 5×10^{-3} eV.

The electronic properties of Au 15 are collected in Table I. The H-L gaps of Au 15 clusters are almost independent of the particle's shape. The values of 0.16–0.18 eV are typical of nonmetallic nanoparticles, but are constantly lower than the gaps found for the previously described clusters. The cohesive energy is increased compared to the smaller clusters.

E. Au 20

Pyramidal $\mathcal{T}_d$ Au 20 (Fig. 11) has been described as a highly stable structure and has been also observed

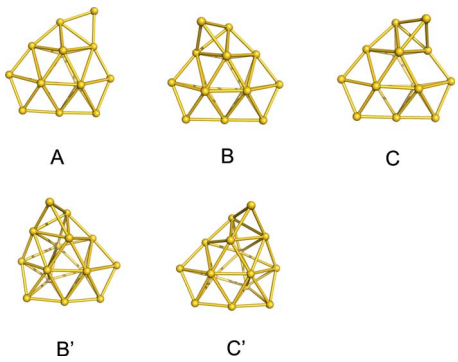

FIG. 10. (Color online) Three dimensional minimum energy structures of Au 15 that are formed during 60 ps of MD at 300 K.

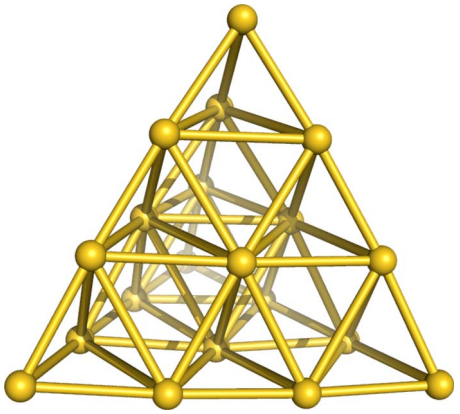

FIG. 11. (Color online) Minimum energy structure of pyramidal Au 20 particle.

experimentally.[70,72,92,93] We have run a dynamic simulation on this structure in the same time frame as for the previous systems (80 ps) and indeed at 300 K the particle activated only its vibrational modes without changing the relative positions of its constituent atoms. Fluxional movements that were observed for the particles studied in the previous paragraphs were not observed. Table I gives the electronic properties of pyramidal Au 20: the H-L gap (1.8 eV) is in agreement with the values reported in literature [1.77 eV (Ref. 92) and 1.9 eV (Ref. 72)], and indicates the great stability of the cluster. The larger cohesive energies within the investigated series is also consistent with a higher stability of this geometry.

F. Au 34

Photoelectron spectra of Au 34^- display a large energy gap between ground state and higher binding energies[38] consistent with the shell closing of neutral Au 34 cluster.[94] This observation is consistent with a particular stability of this cluster. Nonetheless a first principles Car-Parrinello dynamics calculation on gold particles performed for Au 34^- (Ref. 38) revealed a fluxional behavior of the outer shell. The structure was described as a fluxional core-shell cluster with three or four core atoms and a soft shell. The hereby cited contribution did not specify the details of the dynamic simulation, in particular the temperature and the sampled time were not specified. We therefore investigated the neutral Au 34 particle in order to compare this larger system to the smaller ones shown in the previous paragraph and verify its fluxionality. We started the MD from the $\mathcal{C}_3$ Au 34 structure proposed by Wales *et al.*[95] and let the structure evolve. The basin found is represented in Fig. 12 (Cartesian coordinates available as auxiliary material)[69] and is consistent with the minimum energy structures already described for the anion Au 34^-.[38,82] Our results show that the core of 4 Au atoms remains constant during the simulation. No passage to a 3-atom-core was found. This is consistent with the previous results indicating that three and five core structures (found by basin-hopping) lie at higher energies.[38] The mere visual observation of the trajectory for this particle was too complex to simply determine changes in relative atomic positions,

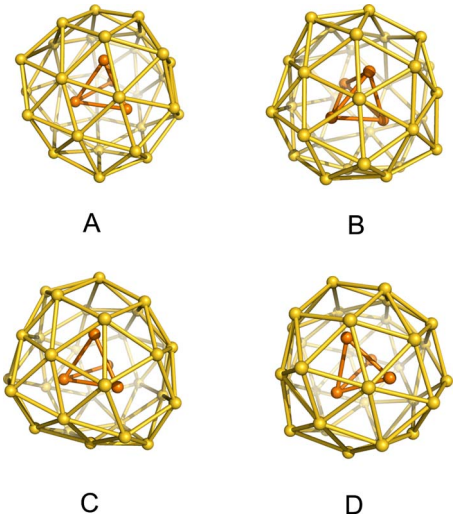

FIG. 12. (Color online) Three-dimensional minimum energy structures of Au 34 that are formed during 60 ps of MD at 300 K. In the color figure (online only) core-shell structures have been evidenced by coloring the core atoms in orange and the shell atoms in yellow.

therefore structural descriptors were used to identify topological features of the particle. The average coordination number between interacting core atoms ($C_{C,C}$), between shell atoms ($C_{S,S}$) and between interacting core and shell atoms ($C_{C,S}$) was determined using the formula given in the Computational Methods section, with a cutoff of 3.4 Å, and the resulting values were as follows: (i) $C_{C,C}$ is 2.66 ± 0.04 Å, (ii) $C_{S,S}$ is 5.80 ± 0.04 Å, and (iii) $C_{C,S}$ is 1.25 ± 0.02 Å (auxiliary material, Fig. 1).[69] These numbers reveal that while core and shell are well self-coordinated, core, and shell behave more independently with respect to one another. $C_{C,C}$ of 2.7 Å is consistent with the tetrahedral nature of the core, while on the shell the atoms are almost coordinated to saturation, but poorly coordinated to the core atoms. On the other hand, the low value of the standard deviations of the $C_{A,B}$ are an indication of the topological stability of the cluster. These observations are confirmed by the analysis of the average distances between interacting core atoms ($d_{C,C}$), shell atoms ($d_{S,S}$), and interacting core and shell atoms ($d_{C,S}$). $d_{C,C}$ value is 2.82 ± 0.04 Å, $d_{S,S}$ is 2.88 ± 0.01 Å while $d_{C,S}$ is 3.04 ± 0.03 Å, also suggesting that core and shell are separate entities. Interestingly fluctuations of the average distances within the shell are smaller than in the core and than between core and shell. This indicates that major structural mobility occurs in the core rather than in the outer shell. This can be attributed to a rather large space available to the core within the shell, which exerts also an influence on the core. Core atoms feel an external potential due to the surface shell that elongates core atomic distances. A plot of the average distances between interacting core atoms and between interacting core and shell atoms during the dynamic simulation Au 34 at 300 K is given in the auxiliary material (Fig. 2).[69] The division between core and shell also appears in recent theoretical and experimental studies on thiolate protected Au nanoparticles.[96–98] Furthermore, the experimental x-ray

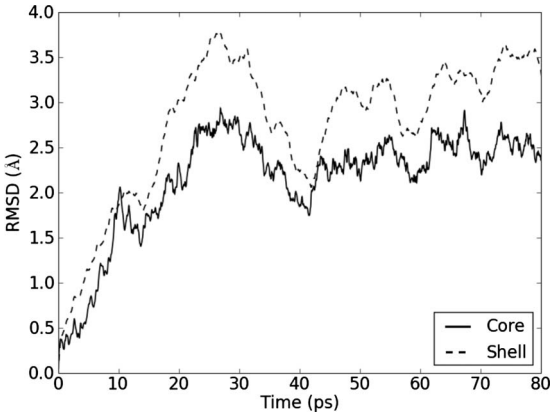

FIG. 13. RMSD of core and shell atoms of Au 34 at 300 K. Changes in the RMSD reflect topological variations within the dynamic simulation thus allowing conformational analysis.

structure of *p*-mercaptbenzoic acid protected Au 102 displays chirality of the Au core.[99]

Identification of local minimum energy structures is also a difficult task by simple visual analysis of the trajectory. We used RMSD to identify structural changes within the trajectory. Figure 13 shows the RMSD of core and shell during the simulation, all calculated with respect to the first frame. The lines behave consistently showing that changes in the core and in the shell occur at the same time. The frames corresponding to local minima and maxima of the curve were isolated and geometry optimization was run on the corresponding structures. This criterion was used to localize the four different local minima shown in Fig. 12(A)–12(D). These four structures are all characterized by a 4 atoms core and a 30 atoms shell, and they are all very close in energy (within K_BT, Table I). The shell shows fluxionality in the change in coordination of the Au atoms (from 5 to 6 and from 6 to 5 with continuity). The shell surface is characterized by triangular and square patterns, characteristic of coordination number 6 and 5, respectively. Such patterns are present in different proportions in each of the structures in Fig. 12. A is characterized by three squares, B is characterized by one square, C is characterized by four squares, and D by two squares. Interestingly the squares are always in correspondence to one of the atoms of the inner tetrahedron and in structure C all four atoms of the core point toward one of the four squares. This can be attributed to the lower coordination present in the square patterns. Table I shows the decreasing of the H-L gap compared to the smaller Au 12 and Au 14 clusters. The electronic structure still deviated from the metallicity of the bulk, but the decrease in H-L gap indicates a trend in the direction of a metallic character. The cohesive energy is linearly increasing compared to the smaller particles.

The relative movement between core and shell has been monitored by following the distance between core and shell atoms. Within a time scale of several picoseconds some bonds are lost and some others are formed, while the rest are kept constant. Examples of the variation in the distances are shown in Fig. 14. It can be thus observed that after 20 ps one atom moves from approximately 3 to approximately 5 Å from the reference atom (Fig. 14, top) while another passes from ca 4.5 Å to ca 3 Å in the same time (Fig. 14, middle). Another atom (Fig. 14, bottom) remains in the original position. It should be noted that interactions between core and shell in core-shell nanoparticles have been shown to be of relevance for the steadiness of photon emission in semiconducting nanoparticles.[100] A simulation at 400 K was performed showing a consistent sampling of the conformational space compared to the MD simulation at 300 K.

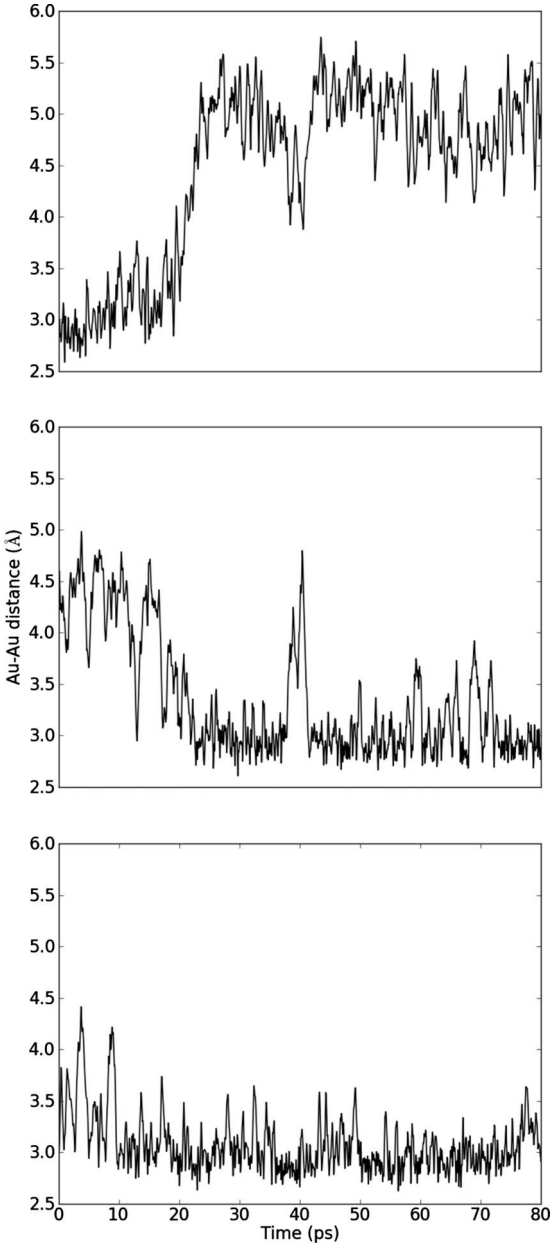

FIG. 14. Formation and breaking of bonds on the shell of the Au 34 particle. The plots show the evolution in time of the distances between three couples of bound Au atoms taken from the outer shell of the particle. The three couples have been chosen to show examples of bond breaking (top), bond formation (middle), and bond retention (bottom) during the dynamic simulation at 300 K.

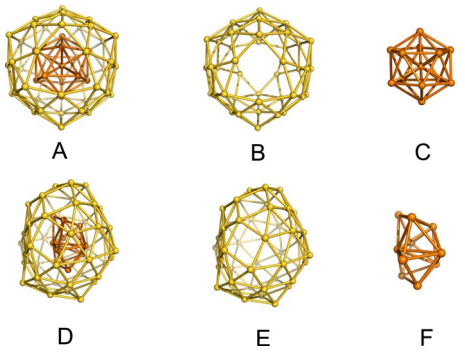

FIG. 15. (Color online) (A) Au 55 after geometry optimization of the icosahedral structure. B and C are, respectively, the shell and the core of structure A. (D) Au 55 after dynamic equilibration and successive geometry optimization. E and F are, respectively, the shell and core of structure D.

G. Au 55

Dynamic simulations on Au 55 particle have also been performed starting from the regular icosahedron. As the regular icosahedron was geometrically optimized it immediately lost its symmetry, reaching a $\mathcal{C}_s$ symmetry as shown in Fig. 15(A) (Cartesian Coordinates of all structures in Fig. 15 are available as auxiliary material).[69] The structure is characterized by the opening of two holes in symmetric positions on the surface. Figures 15(B) and 15(C) show the shell and the core, respectively. As the simulation is run at 300 K after a first equilibration time the $\mathcal{C}_s$ symmetry is lost and a geometric optimization leads to the structure in Fig. 15(D). Figures 15(E) and 15(F) show the shell and the core respectively of the equilibrated structure. The dynamic simulation shows that a similar fluxionality as that observed for Au 34 exists in the outer shell of the equilibrated Au 55 particle. During equilibration (first 10 ps, auxiliary material, Fig. 3)[69] the initial icosahedral core [Fig. 15(C)] loses three atoms and becomes an asymmetric 10 atoms core [Fig. 15(C)] and remains in this form throughout the simulation. Three core atoms therefore become part of the outer shell that passes from 42 to 45 atoms.

The potential-energy profile of the dynamic simulation (Fig. 3 in the auxiliary material)[69] shows that after the first 10 ps the icosahedral structure loses it symmetry and equilibrates to a $\mathcal{C}_1$ (chiral) structure. RMSD analysis of core and shell atoms during the dynamic simulation (auxiliary material, Fig. 4)[69] shows that after a first equilibration period of about 10 ps the structure undergoes only more subtle changes than Au 34, and that as for Au 34 core and shell atoms have different RMSD values. This is the same behavior shown by the Au 13 icosahedral structure which rapidly loses its symmetry. As already noted for Au 34 also the equilibrated Au 55 structure shows a separation between core and shell, which is also well represented by the graphic of the average distances between atoms of the core, atoms of the shell and between interacting core and shell atoms (auxiliary material, Fig. 5).[69] The core atoms, as well as the shell atoms are closer to each other (mean distances are 2.92 ± 0.02 and 2.90 ± 0.01 Å, respectively) than core to surface atoms (3.02 ± 0.02 Å) thus indicating that core and shell also in this case are decoupled to a certain extent.

An interesting feature of the structure in Fig. 15(D) is its chirality. Of course there should be no reason for there being an excess of one enantiomer with respect to the other, but the potential interest of this observation lays in the fact that fluxional gold passes through asymmetric minimum energy structures, which are easily converted one into the other. In principle an external bias (e.g., a chiral ligand), could cause the formation of an excess of one of the enantiomeric forms. This has indeed been experimentally observed by Gautier and Bürgi who were able to detect a vibrational circular dichroism (VCD) adsorption in the region of the gold metal vibrations, when they bound chiral ligands to gold nanoparticles.[88–90] The chiral ligand seemed to be able to preferentially stabilize one of the enantiomeric forms. The formation of chirally enriched nanoparticles is of great potential interest in enantioselective catalysis, since in principle the reaction of prochiral reactants could be performed asymmetrically. Gold nanoclusters with 50–100 atoms are at the interface between metallic and nonmetallic properties and therefore are interesting candidates for further reactivity studies.

H. General overview

A general look at Table I shows that cohesion energies calculated with the relativistic Hamiltonian give throughout the table an increase in about 10% as compared to nonrelativistically corrected ones (fourth column in the table), while the Grimme correction for the dispersion interactions regularly gives an increase in cohesive energy of about 5%. The HOMO-LUMO patterns shown in the table are consistent with the interpretation of the electronic structure of metal clusters given within the jellium spherical shell model and its extensions to shape deformations.[101–105] H-L gaps result larger for closed shells (Au 20 and Au 34) and for even numbers of electrons (Au 12 and Au 14). Furthermore within three-dimensional structures the systems display prolate/oblate deformations to facilitate H-L gap. This is for example the case for Au 13 where all lower symmetry conformations (B, C, D, E, and F, Fig. 1) display larger H-L gaps than the icosahedral structure. In general this effect is smaller than that obtained by spherical shell closing by about one order of magnitude. Shell closing generates H-L of the order of 1 eV, while prolate/oblate deformations give increase in H-L gaps of the order of 0.1 eV.

IV. CONCLUSIONS

The present investigation aims at shedding some light on the fluxional behavior of gold nanoparticles in the picoseconds time scale by means of Born-Oppenheimer molecular dynamics simulations. The dynamic behavior at 300 K of Au_n clusters is complex and for small values of n seems to show peculiar features for each value. Au 12, Au 13, Au 14, and Au 15 clusters have a marked fluxional behavior and oscillate between equilibrium structures according to defined trajectories in phase space. In particular Au 12 and Au 13 rapidly change shape and symmetry, while in Au 14 the eight

outer atoms in the lowest energy structure rotate around the six core atoms. In Au 15 a peripheral atom enters the core structure, and during this process the core structure releases one atom that takes the place of the peripheral. In this way the peripheral atom is continuously exchanged within and without the central part of the particle. Au 20 is especially stable and exhibits no fluxional behavior in the time scale of the simulation. Au 34 and Au 55 have interesting core-shell structures, where core and surface behave to a certain extent as separate elements, with different mobility and different self-coordination. The core has a higher mobility than the surface since it feels the potential of the surface (acting as a cage) while the shell atoms change coordination from 5 to 6 and from 6 to 5 with continuity during the sampled times. The shells of these two larger particles show triangular and square patterns that dynamically change in number and position. The special fluxional behavior of gold nanoparticles investigated by Born-Oppenheimer molecular dynamics showed some of the peculiar features of small gold aggregates which are most likely linked to the reactivity of finely dispersed gold, since fluxionality implies a change in coordination of the metal in the same time scale as that of chemical reactivity, and should in principle allow structural adaptation toward the most favorable free-energy path. Furthermore first principles molecular dynamics is shown to be an elegant method for exploring the conformational three-dimensional complexity of metal nanoparticles, enriching previous structural information with dynamic trajectories that link the different possible topologies.

*Corresponding author; vargas@chem.ethz.ch

[1] F. Baletto and R. Ferrando, Rev. Mod. Phys. **77**, 371 (2005).
[2] C. Burda, X. B. Chen, R. Narayanan, and M. A. El-Sayed, Chem. Rev. **105**, 1025 (2005).
[3] *Metal Nanoparticles: Synthesis, Characterization and Applications*, edited by D. L. Feldheim and C. A. Foss, Jr. (CRC Press, Boca Raton, FL/Taylor & Francis, London, 2002).
[4] P. Pyykko, Angew. Chem. Int. Ed. **43**, 4412 (2004).
[5] P. Pyykko, Inorg. Chim. Acta **358**, 4113 (2005).
[6] P. Pyykko, Chem. Soc. Rev. **37**, 1967 (2008).
[7] H. Hakkinen, Chem. Soc. Rev. **37**, 1847 (2008).
[8] G. J. Hutchings, J. Catal. **96**, 292 (1985).
[9] M. Haruta, T. Kobaiashi, H. Sano, and N. Yamada, Chem. Lett. **16**, 405 (1987).
[10] V. Komanicky, H. Iddir, K. C. Chang, A. Menzel, G. Karapetrov, D. Hennessy, P. Zapol, and H. You, J. Am. Chem. Soc. **131**, 5732 (2009).
[11] A. P. Alivisatos, K. P. Johnsson, X. G. Peng, T. E. Wilson, C. J. Loweth, M. P. Bruchez, and P. G. Schultz, Nature (London) **382**, 609 (1996).
[12] R. P. Andres, T. Bein, M. Dorogi, S. Feng, J. I. Henderson, C. P. Kubiak, W. Mahoney, R. G. Osifchin, and R. Reifenberger, Science **272**, 1323 (1996).
[13] R. L. Whetten, J. T. Khoury, M. M. Alvarez, S. Murthy, I. Vezmar, Z. L. Wang, P. W. Stephens, C. L. Cleveland, W. D. Luedtke, and U. Landman, Adv. Mater. **8**, 428 (1996).
[14] A. P. Alivisatos, Science **271**, 933 (1996).
[15] M. A. El-Sayed, Acc. Chem. Res. **37**, 326 (2004).
[16] P. K. Jain, X. H. Huang, I. H. El-Sayed, and M. A. El-Sayed, Acc. Chem. Res. **41**, 1578 (2008).
[17] S. W. Chen, R. S. Ingram, M. J. Hostetler, J. J. Pietron, R. W. Murray, T. G. Schaaff, J. T. Khoury, M. M. Alvarez, and R. L. Whetten, Science **280**, 2098 (1998).
[18] R. B. Wyrwas, M. M. Alvarez, J. T. Khoury, R. C. Price, T. G. Schaaff, and R. L. Whetten, Eur. Phys. J. D **43**, 91 (2007).
[19] S. J. Oldenburg, J. B. Jackson, S. L. Westcott, and N. J. Halas, Appl. Phys. Lett. **75**, 2897 (1999).
[20] G. Schmid, Chem. Rev. **92**, 1709 (1992).
[21] B. Yoon, P. Koskinen, B. Huber, O. Kostko, B. von Issendorff, H. Hakkinen, M. Moseler, and U. Landman, ChemPhysChem **8**, 157 (2007).
[22] M. Valden, X. Lai, and D. W. Goodman, Science **281**, 1647 (1998).
[23] M. Haruta, S. Tsubota, T. Kobayashi, H. Kageyama, M. J. Genet, and B. Delmon, J. Catal. **144**, 175 (1993).
[24] B. Hammer and J. K. Nørskov, Nature (London) **376**, 238 (1995).
[25] A. Sanchez, S. Abbet, U. Heiz, W. D. Schneider, H. Hakkinen, R. N. Barnett, and U. Landman, J. Phys. Chem. A **103**, 9573 (1999).
[26] M. Mavrikakis, P. Stoltze, and J. K. Nørskov, Catal. Lett. **64**, 101 (2000).
[27] Y. Wang and X. G. Gong, J. Chem. Phys. **125**, 124703 (2006).
[28] G. M. Veith, A. R. Lupini, S. Rashkeev, S. J. Pennycook, D. R. Mullins, V. Schwartz, C. A. Bridges, and N. J. Dudney, J. Catal. **262**, 92 (2009).
[29] J. L. C. Fajin, M. N. D. S. Cordeiro, and J. R. B. Gomes, J. Phys. Chem. C **112**, 17291 (2008).
[30] M. B. Torres, E. M. Fernandez, and L. C. Balbas, J. Phys. Chem. A **112**, 6678 (2008).
[31] B. Yoon, H. Hakkinen, U. Landman, A. S. Worz, J. M. Antonietti, S. Abbet, K. Judai, and U. Heiz, Science **307**, 403 (2005).
[32] I. N. Remediakis, N. Lopez, and J. K. Nørskov, Appl. Catal., A **291**, 13 (2005).
[33] L. M. Molina and B. Hammer, Appl. Catal., A **291**, 21 (2005).
[34] L. M. Molina and B. Hammer, Phys. Rev. Lett. **90**, 206102 (2003).
[35] M. Arenz, U. Landman, and U. Heiz, ChemPhysChem **7**, 1871 (2006).
[36] Z. Y. Li, N. P. Young, M. Di Vece, S. Palomba, R. E. Palmer, A. L. Bleloch, B. C. Curley, R. L. Johnston, J. Jiang, and J. Yuan, Nature (London) **451**, 46 (2008).
[37] P. Koskinen, H. Hakkinen, B. Huber, B. von Issendorff, and M. Moseler, Phys. Rev. Lett. **98**, 015701 (2007).
[38] X. Gu, S. Bulusu, X. Li, X. C. Zeng, J. Li, X. G. Gong, and L. S. Wang, J. Phys. Chem. C **111**, 8228 (2007).
[39] D. Marx and J. Hutter, *Modern Methods and Algorithms of Quantum Chemistry* (John von Neumann Institute for Computing, Jülich, 2000), pp. 301–449.
[40] C. Yannouleas, U. Landman, and R. Barnett, *Metal Clusters* (Wiley, New York, 1999), pp. 145–180.
[41] X. P. Xing, B. Yoon, U. Landman, and J. H. Parks, Phys. Rev. B **74**, 165423 (2006).
[42] C. H. Hu, C. Chizallet, H. Toulhoat, and P. Raybaud, Phys. Rev.

B **79**, 195416 (2009).
[43] S. Iijima and T. Ichihashi, Phys. Rev. Lett. **56**, 616 (1986).
[44] P. M. Ajayan and L. D. Marks, Phys. Rev. Lett. **63**, 279 (1989).
[45] G. Lippert, J. Hutter, and M. Parrinello, Mol. Phys. **92**, 477 (1997).
[46] G. Lippert, J. Hutter, and M. Parrinello, Theor. Chem. Acc. **103**, 124 (1999).
[47] http://cp2k.berlios.de/
[48] E. van Lenthe, E. J. Baerends, and J. G. Snijders, J. Chem. Phys. **99**, 4597 (1993).
[49] E. van Lenthe, E. J. Baerends, and J. G. Snijders, J. Chem. Phys. **101**, 9783 (1994).
[50] E. Baerends, J. Autschbach, A. Bérces, F. Bickelhaupt, C. Bo, P. Boerrigter, L. Cavallo, D. Chong, L. Deng, R. Dickson *et al.*, ADF 2006.01, SCM, Theoretical Chemistry, Vrije Universiteit, Amsterdam, The Netherlands, 2006 available at http:/// www.scm.com/.
[51] J. VandeVondele, M. Krack, F. Mohamed, M. Parrinello, T. Chassaing, and J. Hutter, Comput. Phys. Commun. **167**, 103 (2005).
[52] S. Goedecker, M. Teter, and J. Hutter, Phys. Rev. B **54**, 1703 (1996).
[53] J. VandeVondele and J. Hutter, J. Chem. Phys. **127**, 114105 (2007).
[54] J. P. Perdew, K. Burke, and M. Ernzerhof, Phys. Rev. Lett. **77**, 3865 (1996).
[55] J. VandeVondele and J. Hutter, J. Chem. Phys. **118**, 4365 (2003).
[56] I. Kuo *et al.*, J. Phys. Chem. B **108**, 12990 (2004).
[57] C. G. Broyden, Math. Comput. **24**, 365 (1970).
[58] J. Nocedal, Math. Comput. **35**, 773 (1980).
[59] D. Liu and J. Nocedal, SIAM (Soc. Ind. Appl. Math.) J. Sci. Stat. Comput. **10**, 1 (1989).
[60] D. Shanno and P. Kettler, Math. Comput. **24**, 657 (1970).
[61] D. Goldfarb, Math. Comput. **24**, 23 (1970).
[62] G. Bussi, D. Donadio, and M. Parrinello, J. Chem. Phys. **126**, 014101 (2007).
[63] S. H. Vosko, L. Wilk, and M. Nusair, Can. J. Phys. **58**, 1200 (1980).
[64] E. van Lenthe and E. J. Baerends, J. Comput. Chem. **24**, 1142 (2003).
[65] S. Grimme, J. Comput. Chem. **27**, 1787 (2006).
[66] M. Iannuzzi, A. Laio, and M. Parrinello, Phys. Rev. Lett. **90**, 238302 (2003).
[67] A. Stirling, M. Iannuzzi, A. Laio, and M. Parrinello, ChemPhysChem **5**, 1558 (2004).
[68] M. Sprik, Faraday Discuss. **110**, 437 (1998).
[69] See EPAPS Document No. E-PRBMDO-80-076943 for (1) Cartesian coordinates of the structures of the clusters in the manuscript and (2) additional Figures 1, 2, 3, and 4. For more information on EPAPS, see http://www.aip.org/pubservs/epaps.html.
[70] S. Bulusu, X. Li, L. S. Wang, and X. C. Zeng, Proc. Natl. Acad. Sci. U.S.A. **103**, 8326 (2006).
[71] L. Xiao, B. Tollberg, X. K. Hu, and L. C. Wang, J. Chem. Phys. **124**, 114309 (2006).
[72] A. J. Karttunen, M. Linnolahti, T. A. Pakkanen, and P. Pyykko, Chem. Commun. (Cambridge) **2008**, 465.
[73] J. P. K. Doye and D. J. Wales, New J. Chem. **22**, 733 (1998).
[74] A. P. Sutton and J. Chen, Philos. Mag. Lett. **61**, 139 (1990).
[75] Z. Q. Li and H. A. Scheraga, Proc. Natl. Acad. Sci. U.S.A. **84**, 6611 (1987).
[76] B. Soule de Bas, M. J. Ford, and M. B. Cortie, J. Mol. Struct. THEOCHEM **686**, 193 (2004).
[77] P. Koskinen, H. Hakkinen, G. Seifert, S. Sanna, T. Frauenheim, and M. Moseler, New J. Phys. **8**, 9 (2006).
[78] W. Huang, M. Ji, C. D. Dong, X. Gu, L. M. Wang, X. G. Gong, and L. S. Wang, ACS Nano **2**, 897 (2008).
[79] H. Hakkinen, M. Moseler, O. Kostko, N. Morgner, M. A. Hoffmann, and B. von Issendorff, Phys. Rev. Lett. **93**, 093401 (2004).
[80] F. Furche, R. Ahlrichs, P. Weis, C. Jacob, S. Gilb, T. Bierweiler, and M. M. Kappes, J. Chem. Phys. **117**, 6982 (2002).
[81] A. Lechtken, C. Neiss, M. M. Kappes, and D. Schooss, Phys. Chem. Chem. Phys. **11**, 4344 (2009).
[82] A. Lechtken, D. Schooss, J. R. Stairs, M. N. Blom, F. Furche, N. Morgner, O. Kostko, B. von Issendorff, and M. M. Kappes, Angew. Chem. Int. Ed. **46**, 2944 (2007).
[83] X. Lopez-Lozano, L. A. Perez, and I. L. Garzon, Phys. Rev. Lett. **97**, 233401 (2006).
[84] C. E. Roman-Velazquez, C. Noguez, and I. L. Garzon, J. Phys. Chem. B **107**, 12035 (2003).
[85] I. L. Garzon, M. R. Beltran, G. Gonzalez, I. Gutierrez-Gonzalez, K. Michaelian, J. A. Reyes-Nava, and J. I. Rodriguez-Hernandez, Eur. Phys. J. D **24**, 105 (2003).
[86] I. L. Garzon, J. A. Reyes-Nava, J. I. Rodriguez-Hernandez, I. Sigal, M. R. Beltran, and K. Michaelian, Phys. Rev. B **66**, 073403 (2002).
[87] T. G. Schaaff and R. L. Whetten, J. Phys. Chem. B **104**, 2630 (2000).
[88] C. Gautier and T. Bürgi, J. Am. Chem. Soc. **130**, 7077 (2008).
[89] C. Gautier and T. Bürgi, Chimia (Aarau) **62**, 465 (2008).
[90] C. Gautier and T. Bürgi, ChemPhysChem **10**, 483 (2009).
[91] J. Akola and M. Manninen, Phys. Rev. B **63**, 193410 (2001).
[92] J. Li, X. Li, H. J. Zhai, and L. S. Wang, Science **299**, 864 (2003).
[93] P. Gruene, D. M. Rayner, B. Redlich, A. F. G. van der Meer, J. T. Lyon, G. Meijer, and A. Fielicke, Science **321**, 674 (2008).
[94] K. J. Taylor, C. L. Pettiettehall, O. Cheshnovsky, and R. E. Smalley, J. Chem. Phys. **96**, 3319 (1992).
[95] D. Wales, J. Doye, A. Dullweber, M. Hodges, F. Naumkin, F. Calvo, J. Hernanderz-Rojas, and T. Middletone, The Cambridge Cluster Database, http://www-wales.ch.cam.ac.uk/ccd.html.
[96] M. Walter, J. Akola, O. Lopez-Acevedo, P. D. Jadzinsky, G. Calero, C. J. Ackerson, R. L. Whetten, H. Gronbeck, and H. Hakkinen, Proc. Natl. Acad. Sci. U.S.A. **105**, 9157 (2008).
[97] J. Akola, M. Walter, R. L. Whetten, H. Hakkinen, and H. Gronbeck, J. Am. Chem. Soc. **130**, 3756 (2008).
[98] H. Hakkinen, M. Walter, and H. Gronbeck, J. Phys. Chem. B **110**, 9927 (2006).
[99] P. D. Jadzinsky, G. Calero, C. J. Ackerson, D. A. Bushnell, and R. D. Kornberg, Science **318**, 430 (2007).
[100] X. Y. Wang, X. F. Ren, K. Kahen, M. A. Hahn, M. Rajeswaran, S. Maccagnano-Zacher, J. Silcox, G. E. Cragg, A. L. Efros, and T. D. Krauss, Nature (London) **459**, 686 (2009).
[101] W. Ekardt, Phys. Rev. B **29**, 1558 (1984).
[102] W. Ekardt, Phys. Rev. Lett. **52**, 1925 (1984).
[103] W. Ekardt and Z. Penzar, Phys. Rev. B **38**, 4273 (1988).
[104] M. Manninen, Solid State Commun. **59**, 281 (1986).
[105] M. J. Puska, R. M. Nieminen, and M. Manninen, Phys. Rev. B **31**, 3486 (1985).